Calhoun: The NPS Institutional Archive

DSpace Repository

NPS Scholarship | Publications

2009-01

Transformed flux-form semi-Lagrangian schemes for coastal ocean modeling

Chu, Peter C.; Fan, C.W.

Chu, P.C., and C.-W. Fan, 2009: Transformed flux-form semi-Lagrangian schemes for coastal ocean modeling. Eighth Conference on Coastal Atmospheric and Oceanic Prediction and Process, American Meteorological Society

https://hdl.handle.net/10945/36302

This publication is a work of the U.S. Government as defined in Title 17, United States Code, Section 101. Copyright protection is not available for this work in the United States.

Downloaded from NPS Archive: Calhoun

http://www.nps.edu/library

Calhoun is the Naval Postgraduate School's public access digital repository for research materials and institutional publications created by the NPS community. Calhoun is named for Professor of Mathematics Guy K. Calhoun, NPS's first appointed -- and published -- scholarly author.

Dudley Knox Library / Naval Postgraduate School
411 Dyer Road / 1 University Circle
Monterey, California USA 93943

Proceedings of 8th Conference on Coastal Atmospheric and Oceanic Prediction and Process, Phoenix, 11-15 January 2009

4.5 Transformed Flux-form Semi-Lagrangian Scheme for Coastal Ocean Modeling

Peter C. Chu[1)], and C.W. Fan
Naval Ocean Analysis and Prediction Laboratory
Department of Oceanography
Naval Postgraduate School
Monterey, California

1. Introduction

Numerical approaches in atmospheric and oceanic modeling inevitably introduce diffusion (or dissipation) and dispersion into the approximate solution. From a physical point of view, advection of a passive tracer is the simple transition of a quantity. Therefore, dispersion, the propagation of different spatial scales at different phase speed, and diffusion are processes that are aliens to the process that is being modeled (Chu and Fan 1998, 1999). As applied to constituent advection problem, these numerical artifacts manifest themselves as nonphysical mixing by numerical diffusion, nonphysical highs and lows in the constituent field caused by dispersion, and nonphysical tracer spectra caused by the trapping of tracer in nonpropagating small spatial scales (Rood 1987). The less the numerical diffusion and dispersion errors, the better the model performance is.

Propagation of a Rossby soliton on an equatorial beta-plane is treated as an asymptotic solution, which exists to the inviscid, nonlinear shallow water equations. In principle, the soliton propagates to the west at fixed phase speed, without change of shape. Since the uniform propagation and shape preservation of the soliton are achieved through a delicate balance between linear wave dynamics and nonlinearity. In other words, the Rossby soliton is non-diffusive and non-dispersive (Boyd 1980), which makes it a perfect test case for verification of numerical schemes in ocean models since any diffusion and dispersion in the numerical solution of the Rossby soliton are computational errors. Interested readers are referred to the website: http://marine.rutgers.edu/po/index.php?model=test-problems.

[1)] ***Corresponding author address*: Peter C. Chu, Naval Postgraduate School, Monterey, CA 93943, email: pcchu@nps.edu**

In this study, we first show instability and large diffusion and dispersion errors in numerical solution of the Rossby soliton using the existing schemes such as the upwind, central, and Lax-Wendroff schemes. Then, we present a transformed flux-form semi-Lagrangian (TFSL) scheme, which has explicit form and much less diffusion and dispersion errors. The numerical solution of the Rossby soliton exists even for large Courant numbers.

The rest of paper is organized as follows. Section 2 describes the equatorial Rossby soliton and its usefulness for the ocean model verification. Section 3 shows the failure of the three existing schemes (upwind, central, and Lax-Wendroff) in simulating the equatorial Rossby soliton. Section 4 introduces the TFSL scheme. Section 5 derives the analytical form of the amplification factor of the TFSL-scheme and shows that this factor does not larger than 1 for large Courant number such as 20. Section 6 shows the capability of the TFSL-scheme in simulating the equatorial Rossby soliton. Section 7 presents the conclusions.

2. Rossby Soliton

Let Ω be the angular frequency of earth's rotation and R be the earth radius, and let (x, y) be the spatial coordinates with unit vectors $(\mathbf{i}, \mathbf{j})$ and t be the time. Consider a single layer of homogeneous ocean layer with depth of H. The Lamb's parameter is defined by

$$E = \frac{4\Omega^2 R^2}{gH}, \qquad (1)$$

where g is the gravitational acceleration. The length and time are nondimensionalized by

$$L = \frac{R}{E^{1/4}}, \quad T = \frac{E^{1/4}}{2\Omega}. \qquad (2)$$

Let (x, y) be the non-dimensional Cartesian coordinates, (u, v) be the non-dimensional velocity components in the meridional and

latitudinal directions, and ϕ be the non-dimensional surface elevation. After defining

$$s \equiv x - ct\,, \tag{3}$$

and transforming the nonlinear shallow water wave equations into a frame of reference moving with the linear wave, the flow variables (u, v, ϕ) for the mode-1 can be represented by (Boyd 1980)

$$u(s,y,t) = \frac{(6y^2-9)}{4}\eta(s,t)\exp\left[-\frac{y^2}{2}\right], \tag{4a}$$

$$v(s,y,t) = 2y\frac{\partial \eta(s,t)}{\partial s}\exp\left[-\frac{y^2}{2}\right], \tag{4b}$$

$$\phi(s,y,t) = \frac{(6y^2+3)}{4}\eta(s,t)\exp\left[-\frac{y^2}{2}\right], \tag{4c}$$

and the variable $\eta(s,t)$ satisfies

$$\frac{\partial \eta}{\partial t} - f_1\eta\frac{\partial \eta}{\partial s} - f_2\frac{\partial^3 \eta}{\partial s^3} = 0,$$
$$f_1 = 1.5366, \tag{5}$$
$$f_2 = 0.098765$$

which is the Korteweg-de Vries (KDV) equation with the exact solution,

$$\eta(s,t) = A\,\mathrm{sech}^2\left[B\left(s+\mu B^2 t\right)\right],$$
$$A = 0.772B^2,\ B = 0.394,\ \mu = 0.395\,. \tag{6}$$

Substitution of the exact solution (6) into the third term in the lefthand side of (5) leads to

$$\frac{\partial \eta}{\partial t} - f_1\eta\frac{\partial \eta}{\partial s} = S, \tag{7}$$

$$S(s,t) = 8AB^3 f_2$$
$$\{3\,\mathrm{sech}^4[B(s+\mu B^2 t)]\tanh[B(s+\mu B^2 t)] \tag{8}$$
$$-\mathrm{sech}^2[B(s+\mu B^2 t)]\tanh[B(s+\mu B^2 t)]\},$$

where S is treated as a source/sink term. Evidently equation (7) has the analytical solution (6), and therefore it can be used to verify the stability of the numerical schemes since the diffusion term has been changed into the given source/sink term.

3. Several Existing Schemes

To solve equation (7) numerically, the fluid is assumed to occupy equatorial region around the earth. The zonal direction is discretized into 120 cells (i.e., resolution at 3^o longitude). The depth of fluid is set up as 100 m. The increment Δs is given by

$$\Delta s = \frac{2\pi R}{120L} \approx 0.256\,. \tag{9}$$

The time step is denoted by Δt. Equation (7) can be discretized by the commonly used upwind scheme,

$$\eta_i^{n+1} = \eta_i^n + C_i^n(\eta_{i+1}^n - \eta_i^n) + S_i^n\Delta t\,, \tag{10}$$

the central scheme,

$$\eta_i^{n+1} = \eta_i^n + C_i^n\frac{\eta_{i+1}^n - \eta_{i-1}^n}{2} + S_i^n\Delta t\,, \tag{11}$$

and the Lax-Wendroff scheme,

$$\eta_i^{n+1} = \eta_i^n - \frac{C_i^n}{2}(\eta_{i+1}^n - \eta_{i-1}^n)$$
$$+\frac{(C_i^n)^2}{2}\left(\eta_{i+1}^n - 2\eta_i^n + \eta_{i-1}^n\right) + S_i^n\Delta t, \tag{12}$$

where the superscript and subscript denote the time step and the horizontal grid,

$$\eta_i^n \equiv \eta(x_i, t_n)\,, \tag{13}$$

and

$$C_i^n \equiv \frac{f_1\eta_i^n\Delta t}{\Delta s}\,. \tag{14}$$

In order to compare the difference between numerical and exact solutions (westward propagating Rossby soliton), the zonal equatorial strip is assumed infinitely long. When the Rossby soliton travels over $n\times 120$ cells, it goes around the earth once *n* times (called *n* cycles). The exact solution at $t = 0$ is taken as the initial condition,

$$\eta(s,0) = A\,\mathrm{sec}\,h^2(Bs)\,, \tag{15}$$

with $s = 0$ denoting 0^o longitude.

The three difference equations (10)-(12) are solved numerically from the initial condition (15) representing the upwind, central, and Lax-Wendroff schemes (Lax and Wendroff 1960) with varying Δt at each time step for a given Courant number ($C = 0.75$),

$$\Delta t \equiv \frac{C\Delta s}{f_1\max(|\eta_i^n|)}\,.$$

After obtaining the numerical solution, $\eta(x_i, t_n)$, substituting it into (4c) yields $\phi(s_i, y_j, t_n)$. The accuracy of the schemes can be verified through their capability in predicting the westward propagation of the Rossby soliton. To do so, the surface elevation $\phi(s_i, y_j, t_n)$ is plotted with contour values of 2.13, 4.26, 6.4, 8.53, 10.66, 12,79, 14.93, and 17.06 cm. All the numerical

schemes greatly distort the Rossby soliton (Fig. 1). The numerical solution diverges at 60°45'W using the upwind scheme, and 38°45'W using the central scheme. The numerical solution does not diverge using the Lax-Wendroff scheme, however, the solution is totally different from the analytical solution after propagating one cycle around the earth (comparing Fig. 1d to Fig. 1a).

4. TFSL-Scheme

4.1. Semi-Lagrangian Method

Consider the advection of a passive scalar $\phi(\mathbf{x},t)$ by the velocity **u**(x, *t*). The Eulerian formulation of this is

$$\frac{D\phi}{Dt} \equiv \frac{\partial \phi}{\partial t} + \mathbf{u}\bullet\nabla\phi = S, \qquad (16)$$

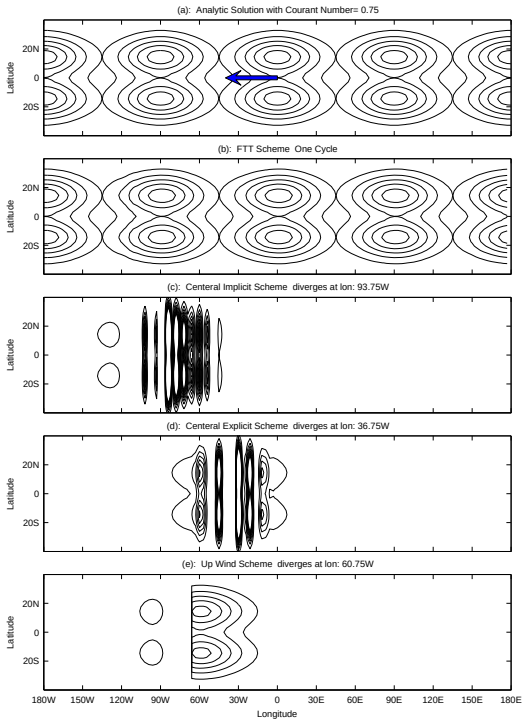

Fig. 1. Surface elevation $\phi(s,y,t)$ of the Rossby solitons obtained from (a) exact solution, and numerical integration with *C* = 0.75 using (b) FTT, (c) implicit central, (d) explicit central, and (e) up wind schemes. Note that the three existing schemes (implicit central, explicit central, up wind) are unstable, but the FTT scheme is stable. The solutions $\phi(s,y,t)$ are plotted at four time instances for the Rossby soliton (exact solution) westward propagating 90°, 180 °, 270°, and 360° (return to the initial location).

where **x** is the position vector, *D*/*Dt* denotes the material derivative, while the Lagrangian counterpart is

$$\frac{d\phi_p}{dt} = S, \qquad \frac{d\mathbf{x}_p}{dt} = \mathbf{u}(\mathbf{x}_p, t)\,. \qquad (17)$$

Here, the subscript '*p*' shows the fluid particle in Lagrangian sense. Although (16) and (17) carry the same physical information, their discretization and numerical implementation is different: (16) is discretized on an Eulerian grid with a finite number of grid points and then time-advanced, while (17) is integrated for a finite number of fluid particles.

Semi-Lagrangian methods combine both Eulerian and Lagrangian points of view: the scalar field is discretized on an Eulerian grid, but is advanced in time using (17). The key element in accomplishing this is the identification of each grid point $\mathbf{x}_i$ as the arrival point, for instance, at $t+\Delta t$, of a particle originating from $\mathbf{x}_i^*$ at time *t*. The algorithm has three steps: (a) the particle associated with each grid point $\mathbf{x}_i$ at time $t+\Delta t$ is traced back to its location $\mathbf{x}_i^*$ at time *t*,

$$\mathbf{x}_i^* = \mathbf{x}_i - \int_t^{t+\Delta t} \mathbf{u}(\tau)\,d\tau\,; \qquad (18)$$

(b) The scalar value at ($\mathbf{x}_i^*$, *t*) is obtained by interpolating the known values at neighboring grid points,

$$\phi(x_i^*, t) = P\left[\phi\{(\hat{\mathbf{x}}_{ik}\}, t\right], \qquad (19)$$

where *P* is any interpolation operator and $\{\hat{\mathbf{x}}_{ik}\}$ denotes the set of interpolation points associated with $\mathbf{x}_i^*$, for example, the nodes of the cell containing $\mathbf{x}_i^*$; (c) Finally, the scalar is updated,

$$\phi(\mathbf{x}_i, t+\Delta t) = \phi(\mathbf{x}_i^*, t) + S_i \Delta t\,. \qquad (20)$$

Thus, the main issues of the semi-Lagrangian method are the backward integration in step (a) and the interpolation in step (b).

4.2. Flux Form

Equation (16) can be rewritten in the flux form with inclusion of diffusion,

$$\frac{\partial \phi}{\partial t} = \nabla\bullet\mathbf{F} + S, \quad \mathbf{F} = -\mathbf{u}\phi + \kappa\nabla\phi\,, \qquad (21)$$

where κ is the diffusion coefficient. Let the dependent variable $\phi(\mathbf{x},t)$ be defined on the space Ω

$$0 \le x \le L_x, \quad 0 \le y \le L_y, \quad 0 \le z \le L_z\,.$$

with (L_x, L_y, L_z) the lengths in (x, y, z) directions. Let

$$\Delta x = \frac{L_x}{N_x},\ \ \Delta y = \frac{L_y}{N_y},\ \ \Delta z = \frac{L_z}{N_z}$$

be the uniform spatial increments with (N_x + 1, N_y + 1, N_z +1) the grid numbers. Integrating (21) for the finite volume,

$$\Delta\Omega_{ijk} = [x_{i-1/2} \le x \le x_{i+1/2},$$

$$y_{j-1/2} \le y \le y_{j+1/2},\ \ z_{k-1/2} \le z \le z_{k+1/2}],$$

$$x_{i\pm1/2} \equiv x_i \pm \Delta x/2,\ \ y_{j\pm1/2} \equiv x_j \pm \Delta y/2,$$

$$z_{k\pm1/2} \equiv z_k \pm \Delta z/2,$$

from t_n to $t_{n+1} = t_n + \Delta t$, we obtain the finite difference equation of the flux-averaged transport,

$$\frac{\tilde{\phi}^{n+1}_{i,j,k} - \tilde{\phi}^{n}_{i,j,k}}{\Delta t} = \frac{\overline{F}^{(n,n+1)}_{i+1/2,j,k} - \overline{F}^{(n,n+1)}_{i-1/2,j,k}}{\Delta x} + \frac{\overline{G}^{(n,n+1)}_{i,j+1/2,k} - \overline{G}^{(n,n+1)}_{i,j-1/2,k}}{\Delta y} + \frac{\overline{H}^{(n,n+1)}_{i,j,k+1/2} - \overline{H}^{(n,n+1)}_{i,j,k-1/2}}{\Delta z} + \hat{S}_{i,j,k}, \quad (22)$$

where (F, G, H) are components of the vector **F**, and

$$\overline{\mathbf{F}}^{(n,n+1)} = \frac{1}{\Delta t}\int_{t_n}^{t_{n+1}} \mathbf{F}dt, \quad (23)$$

represents the temporal average (from t_n to t_{n+1}). The tilde represents the volume average over Ω_{ijk},

$$\tilde{\phi}_{ijk} = \frac{1}{\Delta x\Delta y\Delta z}\iiint_{\Omega_{ijk}} \phi dxdydz. \quad (24a)$$

The hat represents the combined volume (over Ω_{ijk}) and temporal average (from t_n to t_{n+1}),

$$\hat{S}_{ijk} = \frac{1}{\Delta t\Delta x\Delta y\Delta z}\int_{t_n}^{t_{n+1}}\iiint_{\Omega_{ijk}} S dxdydzdt. \quad (24b)$$

For the finite volume $\Delta\Omega_{ijk}$, the flux at x = $x_{i-1/2}$ and $t = t_n$ is calculated by

$$F^{n}_{i-1/2,j,k} = \frac{1}{\Delta y\Delta z}\int_{z_{k-1/2}}^{z_{k+1/2}}\int_{y_{j-1/2}}^{y_{j+1/2}}\left(\kappa\frac{\partial\phi}{\partial x} - u\phi\right)_{x=x_{i-1/2}}^{t=t_n} dydz. \quad (25)$$

To solve equation (22) numerically, we need to compute the temporally integrated fluxes,

$$\overline{F}^{(n,n+1)}_{i+1/2,j,k},\ \ \overline{F}^{(n,n+1)}_{i-1/2,j,k},\ \ \overline{G}^{(n,n+1)}_{i,j+1/2,k},$$

$$\overline{G}^{(n,n+1)}_{i,j-1/2,k},\ \ \overline{H}^{(n,n+1)}_{i,j,k+1/2},\ \ \overline{H}^{(n,n+1)}_{i,j,k-1/2}.$$

If these fluxes are computed using the semi-Lagrangian method, it is called the flux-form semi-Lagrangian scheme (Lin and Rood 1996).

4.3. Transformation of Temporal into Spatial Mean

For simplicity and no loss of generality, we consider one dimensional problem of (22) without source/sink term (i.e., $\hat{S}_{ijk}$ = 0),

$$\frac{\tilde{\phi}^{n+1}_i - \tilde{\phi}^{n}_i}{\Delta t} = \frac{\overline{F}^{(n,n+1)}_{i+1/2} - \overline{F}^{(n,n+1)}_{i-1/2}}{\Delta x}. \quad (26)$$

From the semi-Lagrangain consideration, we have

$$\tilde{\phi}(x^*_i, t_n) = \tilde{\phi}(x_i, t_n) + \frac{[\overline{F}^{(n,n+1)}_{i+1/2} - \overline{F}^{(n,n+1)}_{i-1/2}]\Delta t}{\Delta x}. \quad (27)$$

Using the characteristic-line concept, the flux at time step t_{n+1} and location $x_{i\text{-}1/2}$ can be transformed into the flux at time step t_n and location $x_{i\text{-}1/2\text{-}C}$ (Fig. 2),

$$F^{n+1}_{i-1/2} = F^{n}_{i-1/2-C}, \quad (28)$$

and the temporally averaged flux $\overline{F}^{(n,n+1)}_{i-1/2}$ [similar for $\overline{F}^{(n,n+1)}_{i+1/2}$] can be transformed into spatial averaged flux,

$$\overline{F}^{(n,n+1)}_{i-1/2} \equiv \frac{1}{\Delta t}\int_{t_n}^{t_n+\Delta t} F\left(x_{i-1/2}, t\right)dt = \frac{1}{C\Delta t}\int_{x_{i-1/2}-c\Delta t}^{x_{i-1/2}} F\left(x, t_n\right)dx. \quad (29)$$

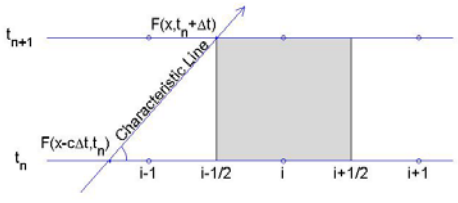

Fig. 2. Temporally varying flux at the boundary $x_{i\text{-}1/2}$ from t_n to t_n + Δt is transformed into spatially varying flux at t n from $x_{i\text{-}1/2}$ - $C\Delta t$ to $x_{i\text{-}1/2}$ using the characteristic-line concept.

where

$$C = u\Delta t / \Delta x, \qquad (30)$$

is the Courant number. Substitution of (30) into (29) leads to

$$\overline{F}_{i-1/2}^{(n,n+1)} \approx \begin{cases} (F_{i-1/2}^n + F_{i-1/2-C}^n)/2 & \text{if } C \le \frac{1}{2} \\ \delta_{1/2}\left(F_{i-1/2}^n + F_{i-1}^n\right)/2 & \\ +[\sum_{k=1}^{m-1}\delta_k\left(F_{i-k}^n + F_{i-k-1}^n\right) & \\ +\delta_m\left(F_{i-m}^n + F_{i-1/2-C}^n\right)]/2 & \text{if } C > \frac{1}{2} \end{cases} \qquad (31)$$

where

$$m = \left[C - \frac{1}{2}\right],$$

$$\delta_{1/2} = \frac{1}{2C}, \quad \delta_k = \frac{1}{C}, \quad \delta_m = 1 - \delta_{1/2} - \sum_{k=1}^{m-1}\delta_k . \qquad (32)$$

The bracket [ ] represents the round-off integer. Similarly, the temporally averaged flux at the right boundary ($x = x_{i+1/2}$)

$$\overline{F}_{i+1/2}^{(n,n+1)} \approx \begin{cases} (F_{i+1/2}^n + F_{i+1/2-C}^n)/2 & \text{if } C \le \frac{1}{2} \\ \delta_{1/2}\left(F_{i+1/2}^n + F_i^n\right)/2 & \\ +[\sum_{k=1}^{m-1}\delta_k\left(F_{i-k+1}^n + F_{i-k}^n\right) + & \\ \delta_m\left(F_{i+1-m}^n + F_{i+1/2-C}^n\right)]/2 & \text{if } C > \frac{1}{2} \end{cases} \qquad (33)$$

The temporally averaged fluxes $\overline{F}_{i-1/2}^{(n,n+1)}$ and $\overline{F}_{i+1/2}^{(n,n+1)}$ (from t_n to $t_n + \Delta t$) is transformed into the spatially averaged ones over multiple grids at time step t_n with weights of $\delta_{1/2}, \delta_1, ..., \delta_m$. If the characteristic line at t_n is beyond the boundary, the boundary condition can be used to calculate $\overline{F}_{i-1/2}^{(n,n+1)}$ (Fig. 3),

$$\overline{F}_{3/2}^{(n,n+1)} = \frac{\frac{1}{2}\left(F_1^n + F_{3/2}^n\right) + \left(C - \frac{1}{2}\right)\left(F_b^n + F_1^n\right)}{2C}, \qquad (34)$$

where F_b^n is the boundary value between F_1^n and F_1^{n+1}, and is interpolated by

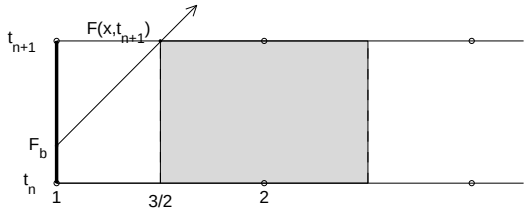

Fig. 3. Same as Fig. 2 except at the left boundary of the integration domain.

$$F_b^n = \left(1 - \frac{1}{2C}\right)F_1^{n+1} + \frac{1}{2C}F_1^n . \qquad (35)$$

Substitution of (31) and (33) into the difference equation (26) leads to

$$\phi_i^{n+1} = \phi_i^n + \begin{cases} -\frac{C}{2}\left(\phi_{i+1}^n - \phi_{i-1}^n\right) & \\ +\frac{C^2}{2}\left(\phi_{i+1}^n - 2\phi_i^n + \phi_{i-1}^n\right), & C \le \frac{1}{2} \\ -\frac{1}{4}\left(\phi_{i+1}^n - \phi_{i-1}^n\right) - & \\ \frac{1}{2}\left(\phi_i^n + \phi_{i-1}^n - \phi_{i-m}^n - \phi_{i-m-1}^n\right) & \\ -\left(D - \frac{D^2}{2}\right)\left(\phi_{i-m}^n - \phi_{i-m-1}^n\right) & \\ -\frac{D^2}{2}\left(\phi_{i-m-1}^n - \phi_{i-m-2}^n\right) & \\ +\frac{1}{8}\left(\phi_{i+1}^n - 2\phi_i^n + \phi_{i-1}^n\right), & C > \frac{1}{2} \end{cases} \qquad (36)$$

which is called the Transformed Flux-formed Semi-Lagrangian (TFSL) scheme for the advection-diffusion equation (21). Here,

$$D = C - m - 1/2 .$$

For $C \le 1/2$, the TFSL scheme is the same as the Lax-Wendroff scheme. Comparing to the central difference (CED), the TFSL-scheme has an extra positive term,

$$\text{TSF-CED} = \frac{C^2}{2}\left(\phi_{i+1}^n - 2\phi_i^n + \phi_{i-1}^n\right), \qquad (37)$$

for $C \le 1/2$. This term can be regarded as the numerical (positive) diffusion which leads to computational stability. Different schemes have different algorithms to compute the temporally averaged fluxes $\overline{F}_{i-1/2}^{(n,n+1)}$ and $\overline{F}_{i+1/2}^{(n,n+1)}$ (from t_n to $t_n + \Delta t$). The TFSL scheme has second order accuracy in both time and space.

5. Stability of the TFSL Scheme

Stability of numerical schemes is an important issue in solving the advection equation (16). In Section 3, we showed the instability of the existing schemes (upwind, central, and Lax-Wendroff). To determine the stability of the TFSL scheme (36), the Fourier series expansion is used. Decay or growth of an amplification factor indicates whether or not the numerical algorithm is stable (von Neumann and Richtmyer 1950). Assuming that at any time step t_n, the compute solution ϕ_i^n is the sum of the exact solution $\phi_i^{n(ex)}$ and error ε_i^n,

$$\phi_i^n = \phi_i^{n(ex)} + \varepsilon_i^n, \qquad (38)$$

and substituting (38) into (36), we obtain

$$\varepsilon_i^{n+1} = \varepsilon_i^n + \begin{cases} -C(\varepsilon_{i+1}^n - \varepsilon_{i-1}^n)/2 \\ +C^2(\varepsilon_{i+1}^n - 2\varepsilon_i^n + \varepsilon_{i-1}^n)/2, & C \le 1/2 \\ -(\varepsilon_{i+1}^n - \varepsilon_{i-1}^n)/4 \\ -(\varepsilon_i^n + \varepsilon_{i-1}^n - \varepsilon_{i-m}^n - \varepsilon_{i-m-1}^n)/2 \\ -(D - D^2/2)(\varepsilon_{i-m}^n - \varepsilon_{i-m-1}^n) \\ -D^2(\varepsilon_{i-m-1}^n - \varepsilon_{i-m-2}^n)/2 \\ +(\varepsilon_{i+1}^n - 2\varepsilon_i^n + \varepsilon_{i-1}^n)/8, & C > 1/2 \end{cases} \qquad (39)$$

The finite mesh function, ε_i^n, can be decomposed into a Fourier series,

$$\varepsilon_i^n = \sum_{j=-N_x}^{N_x} a_j^n \exp(Ii\theta), \quad \theta = j\pi / N_x \qquad (40)$$

with $I \equiv \sqrt{-1}$, (a_j^n, θ) being the amplitude and phase angle of the jth harmonic. Substituting (40) into (39) yields

$$a^{n+1} = g(\theta, C)a^n, \qquad (41)$$

where

$$g(\theta,C) = \begin{cases} 1 - C^2(1-\cos\theta) - IC\sin\theta, & C \le \frac{1}{2} \\ \frac{1}{4}(1-\cos\theta) + \left(\frac{1}{2} - D + \frac{D^2}{2}\right)\cos(m\theta) + \\ \left(\frac{1}{2} + D - D^2\right)\cos[(m-1)\theta] \\ +\frac{D^2}{2}\cos[(m-2)\theta] \\ -I\{(\frac{1}{2} - D + \frac{D^2}{2})\sin(m\theta) \\ +(\frac{1}{2} + D - D^2)\sin[(m-1)\theta] \\ +\frac{D^2}{2}\sin[(m-2)\theta]\}, & C > \frac{1}{2} \end{cases} \qquad (42)$$

is called the amplification factor, whose magnitude is given by

$$|g(\theta,C)|^2 = \begin{cases} [1 - C^2(1-\cos\theta)]^2 + C^2\sin^2\theta, & C \le \frac{1}{2} \\ \frac{1}{16}(1-\cos\theta)^2 + (\frac{1}{2} - D + \frac{D^2}{2})^2 \\ +(\frac{1}{2} + D - D^2)^2 + \frac{D^4}{4} \\ +\frac{1}{2}(1-\cos\theta)\{(\frac{1}{2} - D + \frac{D^2}{2})\cos(m\theta) \\ +(\frac{1}{2} + D - D^2)\cos[(m-1)\theta] \\ +\frac{D^2}{2}\cos[(m-2)\theta]\} \\ +(1 - 2D + 2D^2)(\frac{1}{2} + D - D^2)\cos\theta \\ +D^2(\frac{1}{2} - D + \frac{D^2}{2})\cos(2\theta), & C > \frac{1}{2} \end{cases} \qquad (43)$$

The TFSL-scheme is computationally stable if $|g(\theta,C)| \le 1$ and computationally unstable if $|g(\theta,C)| > 1$. Fig. 4 shows that $|g(\theta,C)| \le 1$ for all θ and C (larger than 20), which implies that the TFSL-scheme (36) is very stable.

6. Simulating the Rossby Soliton Using the TFSL Scheme

The TFSL-scheme (36) is only for spatially variant and temporally invariant *u*.

When u [or $-f_1\eta$ in (7)] at $x_{i\text{-}1/2}$ varies with time from t_n to t_{n+1}, concept of variant characteristic lines can be used to determine $u(x_{i\text{-}1/2}, t)$ with sub time-steps ($\delta t_{1/2}, \delta t_1, ..., \delta t_m$) (between t_n and t_{n+1}) from $u(x, t_n)$ at grid points ($x_{i\text{-}1}, \ldots, x_{i\text{-}m}, x_{i*}$), and for $u > 0$ the time from the left neighboring grid $x_{i\text{-}[k+1]}$ to $x_{i\text{-}k}$ is given by (Fig. 5),

$$\delta t_k = \int_{x_{i-[k+1]}}^{x_{i-k}} \frac{dx}{u(x,t_n)} = \frac{\Delta x}{u^n_{i-k}} \int_0^1 \frac{dz}{1-\zeta_{i-k} z} =$$

$$-\frac{\Delta t}{C_{i-k}} \frac{\ln(1-\zeta_{i-k})}{\zeta} = \frac{\Delta t}{C_{i-k}} (1 + \frac{\zeta_{i-k}}{2} + \frac{\zeta^2_{i-k}}{3} + ...),$$

$$k = 0.5,\ 1,\ 2, ..., m. \tag{44}$$

where

$$\Delta x = x_{i-k} - x_{i-[k+1]},$$

$$\zeta_{i\text{-}k} = \frac{u^n_{i-k} - u^n_{i-[k+1]}}{u^n_{i-k}}, \tag{45}$$

$$C_{i-k} = \frac{u^n_{i-k} \Delta t}{\Delta x}.$$

The parameter $C_{i\text{-}k}$ is the Courant number for sub time steps. A formula similar to (44) can be obtained for $u < 0$ (using the right neighboring grid). The temporally averaged fluxes from t_n to $t_n + \Delta t$ can be calculated by (taking $\overline{F}^{(n,n+1)}_{i-1/2}$ [see (31)] as the example)

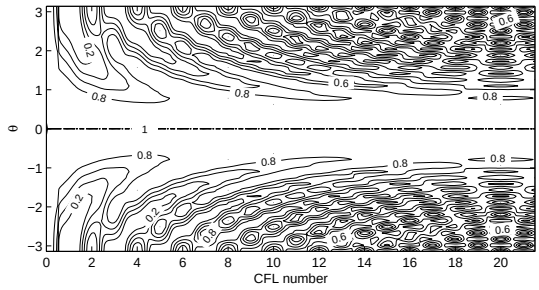

Fig. 4. Dependence of the amplification factor $|g(\theta, C)|$ of the TSFL scheme on θ and C.

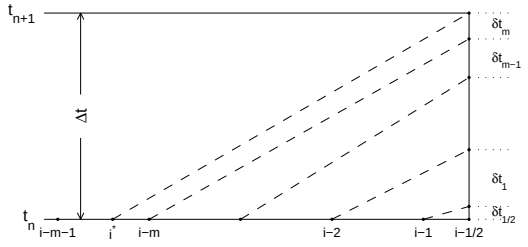

Fig. 5. Same as Fig. 2 except for temporally varying u.

$$\overline{F}^{(n,n+1)}_{i-1/2} = \frac{1}{\Delta t}[\delta t_{1/2} \frac{(F_{i-1/2} + F_{i-1})}{2} + \delta t_1 \frac{(F_{i-1} + F_{i-2})}{2}$$

$$+ ... + \delta t_{m-1} \frac{(F_{i-m+1} + F_{i-m})}{2} + \delta t_m \frac{(F_{i-m} + F^*_{i-m-1})}{2}] \tag{46}$$

Equation (7) for the Rossby soliton is discretized using the flux form,

$$\frac{\eta^{n+1}_i - \eta^n_i}{\Delta t} = \frac{\overline{F}^{(n,n+1)}_{i+1/2} - \overline{F}^{(n,n+1)}_{i-1/2}}{\Delta s} + \hat{S}_i, \tag{47}$$

where $\hat{S}_i$ is the temporally-spatially averaged source term

$$\hat{S}_i \equiv \frac{1}{\Delta t \Delta s} \int_{t_n}^{t_{n+1}} \int_{s_{i-1/2}}^{s_{i+1/2}} S(s,t) ds dt. \tag{48}$$

with $S(s, t)$ given by (8). The difference equation (47) is solved numerically from the initial condition (15) using the TFSL-scheme. To compare with the existing schemes (upwind, central, and Lax-Wendroff schemes), the Courant number is set to 0.75. After the numerical solution $\eta(x_i, t_n)$ is obtained, substituting it into (4c) yields $\phi(s_i, y_j, t_n)$, as shown in Fig. 6. Note that the three existing schemes (upwind, central, and Lax-Wendroff) are all unstable (Fig. 1), but the TFSL-scheme is stable. After propagating westward around the earth the numerical Rossby soliton (using the TFSL scheme) shows almost non-difussive and non-dispersive.

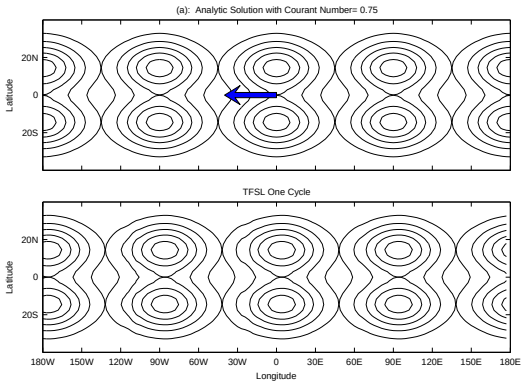

Fig. 6. Surface elevation $\phi(s, y, t)$ of the Rossby soliton obtained from (a) exact solution, and numerical integration with C = 0.75 using (b) TFSL-scheme. The solutions $\phi(s, y, t)$ are plotted at four time instances for the Rossby soliton (exact solution) westward propagating 90°, 180 °, 270°, and 360° (return to the initial location).

To show the quality of the TFSL-scheme, the difference equation (47) is integrated for C = 1.5 for a long time period corresponding to the Rossby soliton propagates westward around the earth 5 times. The solution $\phi(s_i, y_j, t_n)$ is stable all the time (Fig. 7). The relative root-mean-square error (rrmse),

$$\text{rrmse}(t) = \frac{\sqrt{\frac{1}{N_s N_y}\sum_{i=1}^{N_s}\sum_{j=1}^{N_y}\left[\phi^{(num)}(s_i, y_j, t) - \phi^{(ex)}(s_i, y_j, t)\right]^2}}{\max\left|\phi^{(ex)}(s_i, y_j, t)\right|} \tag{49}$$

is calculated to illustrate the accuracy of the TFSL scheme. Table 1 shows RRMSE at the end of first five cycles around the earth. The error varies from 2.66% for the first cycle to 3.53% for the fifth cycle.

Table 1. RRMSE of the surface elevation predicted using the TFSL-scheme after the first five cycles around the earth.

Cycle	1	2	3	4	5
RRMSE (%)	2.66	2.86	3.00	3.22	3.53

7. Conclusions

(1) This study shows that TFSL scheme is a promising stable and accurate scheme for solving the advection-diffusion equation. Magnitude of the amplification factor does not exceed 1 for large Courant number (e.g., for C = 20). The Fourier analysis shows that the TFSL scheme has second-order accuracy in time and space. Computational stability and higher accuracy than the widely used schemes (central, upwind, and Lax-Wendroff) makes this scheme useful in ocean modeling, computational fluid dynamics, and numerical weather prediction.

(2) Several major features distinguish the TFSL scheme from the existing schemes, both Eulerian and semi-Lagrangian. First, the flux (F) at the boundary of each grid cell is computed not from a single time step (present or next) but from temporal integration from present to next time step. Second, this temporal integration is transformed into spatial integration at the present time step using the characteristic line method.

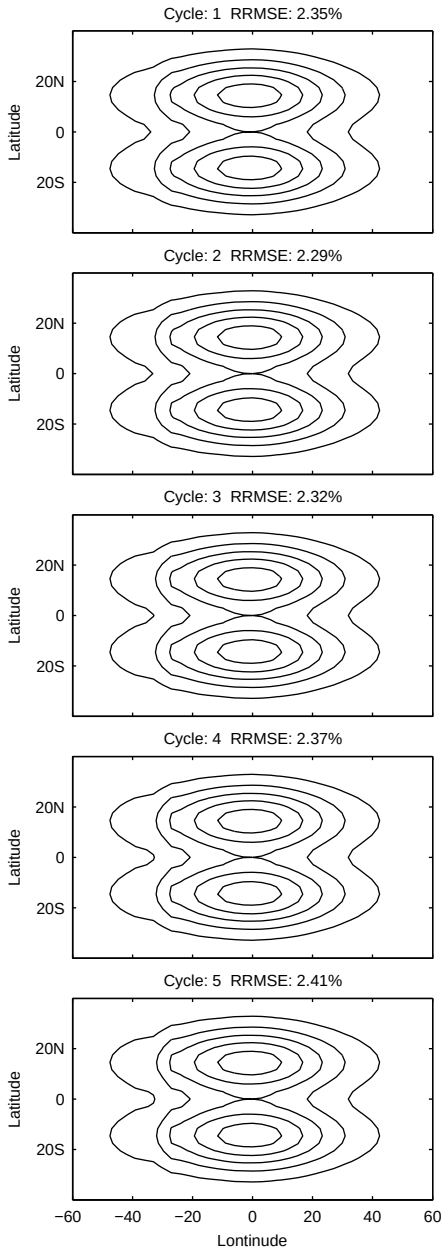

Fig. 7. Surface elevation $\phi(s, y, t)$ of the Rossby soliton after 1-5 cycles around the earth obtained from numerical integration with C = 1.5 using the TFSL scheme.

(3) The equatorial Rossby soliton is used to test the capability of the TFSL scheme since it has exact solution. The equation is solved numerically from the soliton initially located at the equator and 0° longitude with the overall Courant number of 0.75. The existing numerical schemes greatly distort the Rossby soliton and diverge as it propagates: 60°45'W (upwind), 38°45'W (central), and totally distorted after one cycle around the earth (Lax-

Wendroff). However, the TFSL scheme does not distort the Rossby soliton and converge as it propagates many cycles around the earth.

(4) Future studies include applying TFSL scheme to non-uniform grid systems as well as designing higher order TFSL schemes.

Acknowledgments

The Office of Naval Research, the Naval Oceanographic Office, and the Naval Postgraduate School supported this study.

References

Boyd, J.P., 1980: Equatorial solitary waves. Part-1: Rossby Solitons. *Journal of Physical Oceanography*, **10**, 1699-1717.

Chu, P.C., and C.W. Fan, 1998: A three-point combined compact difference scheme. *Journal of Computational Physics*, **140**, 370-399.

Chu, P.C., and C.W. Fan, 1999: A three-point non-uniform combined compact difference scheme. *Journal of Computational Physics*, **148**, 663-674.

Lax, P., and B. Wendroff, 1960: Systems of conservation laws. *Communication on Pure and Applied Mathematics*, **13**, 217-237.

Lin S., and R. B. Rood, 1996: Multidimensional flux-form semi-Lagrangian transportation schemes. *Monthly Weather Review*, **124**, 2046–2070.

Rood, R. B., 1987: Numerical advection algorithms and their role in atmospheric transport and chemistry models. *Review of Geophysics*, **25,** 71–100.

von Neumann, J., and R.D. Richtmyer, 1950: A method for the numerical calculation of hydrodynamic shocks. *Journal of Applied Physics*, **21**, 232.